Strain Measurement in Coilable Thin Composite Shells with Embedded Fiber Bragg Grating Sensors

Brayden Aller* and Sergio Pellegrino†
California Institute of Technology, Pasadena, CA, 91125

Nathan Kinkaid‡, Juan Mejia-Ariza§, and Richard Otis¶
Jet Propulsion Laboratory (JPL), California Institute of Technology, Pasadena, CA, 91109

Patrick Hon Man Chan‖ and Francisco Pena**
NASA Armstrong Flight Research Center (AFRC), Edwards, CA, 93523

Progress towards the use of ultra-thin fiber Bragg grating sensors for the in-situ strain measurement of coilable thin composite shells is presented. The first part of this work presents the manufacturing procedure used in the construction of these composite shells with embedded sensors. The second part of this work investigates how embedded ultra-thin fiber Bragg grating sensors affect the bending stiffness and failure curvature of these laminates through the use of the column bending test. The influence of the embedded sensors on the failure of these laminates is further investigated through μCT imaging after failure.

I. Introduction

Large-area spacecraft constructed of thin composite shells are tightly coiled to fit into the launch vehicle before their deployment in space. While coiled, thin composites can undergo changes that negatively impact their performance upon deployment. These include time-dependent failure and rupture from being held in a high strain state [1] as well as damage to the structure induced by inter-layer slip under launch vibrations [2]. To ensure the integrity of these structures throughout their mission-life, it is of interest to measure their internal strain state and detect changes over time. Fiber Bragg grating (FBG) sensors are a promising approach to such measurements due to their small profile, light weight and distributed sensing capability. FBG sensors are a type of optical fiber sensor in which gratings are inscribed within the fiber core that reflect a single wavelength of light. This wavelength, λ, is proportional to both the effective refractive index of the optical fiber, n, and the grating period, Λ via

$$\lambda = 2n\Lambda \tag{1}$$

As a strain or temperature change is applied to an FBG, a shift in λ will occur. These shifts can be tracked over time and converted into either a temperature or strain measurement according to the expression

$$\frac{\Delta\lambda}{\lambda_0} = \alpha\varepsilon + \beta\Delta T \tag{2}$$

where λ_0 is the value of λ of the baseline configuration we are measuring changes from, $\Delta\lambda$ is the measured change in reflected wavelength from baseline, α is the gage factor, ε is the fiber strain, β is the thermo-optic coefficient, and ΔT is the change in temperature.

Strain sensing of composite laminates using embedded FBG sensors has been extensively studied with examples ranging from the tracking of residual strain buildup during curing [3], to the detection of transverse cracking [4] and

---

*Graduate Student, Graduate Aerospace Laboratories, 1200 E California Blvd, MC 105-50, AIAA Student Member. baller@caltech.edu

†Joyce and Kent Kresa Professor of Aerospace and Civil Engineering, Graduate Aerospace Laboratories, 1200 E California Blvd, MC 105-50, AIAA Fellow. sergiop@caltech.edu

‡Mechanical Engineer, Spacecraft Mechanical Engineering, 4800 Oak Grove Dr.

§Technologist and Instructor of Advanced Composite Structures; Materials Development, Testing and Failure Investigations Group, 4800 Oak Grove Dr., AIAA Senior Member

¶Technologist, Materials Development and Manufacturing Technology, 4800 Oak Grove Dr.

‖Electronics Engineer, Advanced Systems Development Branch, P.O. Box 273, Edwards, California

**Aerospace Engineer, Aerostructures Branch, P.O. Box 273, Edwards, California, AIAA Member

delamination [5], to even the measurement of internal strains under bending [6]. However, all of this previous research deals with composite laminates much thicker than those used in coilable composite shells ($\leq 200~\mu$m). In general, the smaller the diameter of the embedded FBG sensor, the smaller the disruption to the laminate microstructure.

To enable inclusion into these thin composite shells with minimal disruption to the laminate, very small diameter FBG sensors are needed. The most common FBG sensors have a cladding diameter of 125 μm and usually an additional protective polymer coating, making them far too thick to use in coilable composite shells. In our previous work, where we demonstrated the ability of FBG sensors to measure coiling strains in thin composite laminates [7], we were able to use FBG sensors with a total diameter of 71 μm, which at the time were the smallest available. To ensure complete consolidation of the carbon fibers around the embedded sensor, the lamina in which the sensor is embedded should be at least as thick as the embedded fiber itself. The diameter of our previous FBG sensors greatly restricts their use in coilable thin composite shells. In the present work, we were able to get custom-made ultra-thin FBG sensors with a cladding diameter of only 30 μm, making them perfectly suited for strain sensing in structures constructed of coilable thin composite shells. To the best of the authors' knowledge, these are the smallest diameter FBG sensors to have been used in composites, with the previous smallest having a cladding diameter of 40 μm and a coating of 52 μm [8].

The goal of this paper is to present our progress towards the use of ultra-thin FBG sensors for the in-situ strain measurement of coilable thin composite shells. To this end, the paper is split into two parts. The first part discusses the FBG embedment procedure and shows results from an initial embedment of one of these FBGs in a coilable thin composite shell. The second part investigates how the the embedment of these FBG sensors and their position within the laminate affect the bending behavior of these thin shells through the use of the column bending test and μCT imaging.

II. Manufacturing of Coilable Composite Shells with Embedded FBGs

The ultra-thin FBG sensors used in this work were procured from Redondo Optics, Inc. These FBGs were constructed using custom 30 μm cladding diameter optical fiber with an acrylate coating, which served to protect the fiber during handling. This coating was removed from the embedded region prior to embedment to reduce the total diameter of the FBG sensor and minimize its intrusion into the laminate. The acrylate coating was carefully burned off with a lighter and it was found that using a lower temperature part of the flame helped prevent fiber warping and the degradation of the FBG while still cleanly removing the coating. For this work, the coilable thin composite shells were constructed out of 30 grams per square meter (gsm) unidirectional carbon fiber prepreg with NTPT ThinPreg 402 epoxy resin and T800 carbon fibers with a layup of [0_2/90_2/0_2] yielding a total cured thickness of approximately 200 μm. In these laminates, the fibers were embedded in the outer $0°$ lamina to offset the sensor from the mid-surface to enable the measurement of bending strains. The FBG sensor was aligned with the carbon fibers to enable good fiber consolidation around the sensor and to minimize the intrusion of the FBG in the laminate. To ensure a uniform surface finish on both sides of the laminates, polyimide membrane with mold release was placed on both sides and removed after curing. A cross-sectional μCT image of one of these laminates with the embedded ultra-thin fiber can be seen in Fig. 1. This image was taken with a ZEISS XRadia 510 Versa 3D X-ray microscope.
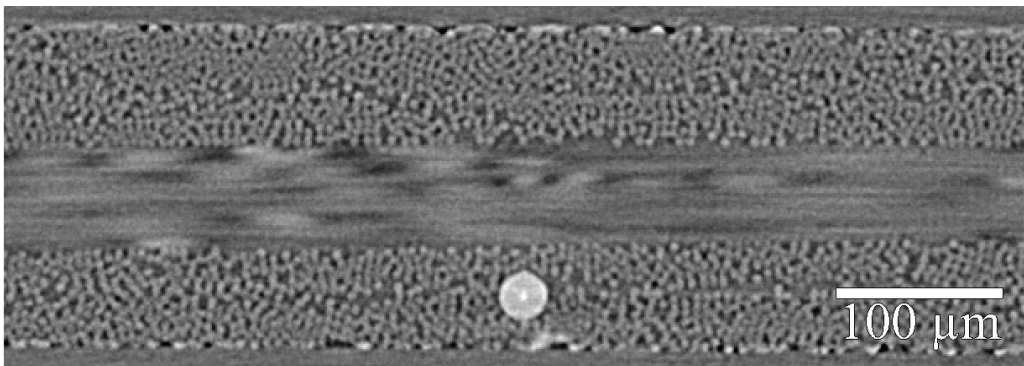

Fig. 1 μCT scan of [0_2/90_2/0_2] laminate with embedded fiber.

An ultra-thin FBG was successfully embedded in the [0_2/90_2/0_2] laminate, which was chosen as it enables the complete consolidation of the carbon fibers around the entire diameter of the FBG as can be seen in Fig. 1. Throughout the manufacturing and embedment process, full spectrum readings of this grating were taken using a Luna HYPERION

si255 interrogator. Typical FBG sensors reflect a singular peak in the spectral domain, the center of which is the wavelength λ that is tracked in the measurement of strain. In this case, the initial FBG spectrum was distorted and a clear singular peak could not be found. This issue is expected to be resolved in future batches of sensors. Two of these full spectrum measurements are presented in Fig. 2 illustrating the measured FBG spectra before and after it was embedded into the laminate. It can be seen that while the spectrum was already distorted before, the general profile did not appear to distort further and instead shifted to the left likely indicating the presence of a compressive strain on the fiber. This is a promising initial result as it indicates that embedment of FBG sensors into these thin laminates likely won't induce any significant FBG spectral distortions that could potentially impede the measurement of strain.
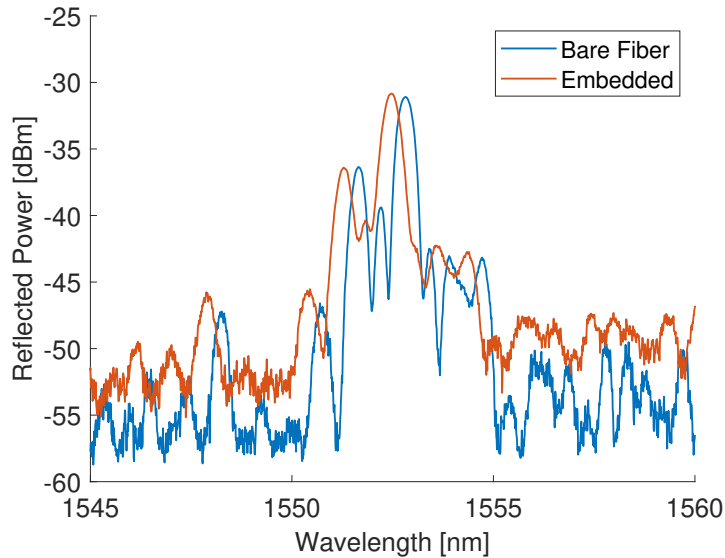

Fig. 2   FBG spectra before and after embedment into thin laminate.

III. Bending Characterization of Coilable Composite Shells with Embedded FBGs

A. Experimental Setup

In coilable thin composite shells, the primary deformation mode is bending as these structures are coiled and stowed prior to deployment. Therefore, it is important to understand and study how these embedded sensors affect the bending behavior of these structures. To do this, the column bending test (CBT) was used in conjunction with two digital image correlation (DIC) systems to measure both the bending stiffness and failure curvature of these thin shells. The experimental setup used for all testing in this is work is depicted in Fig. 3. The CBT fixture was mounted in an Instron load frame with a 500 N load cell. On either side of the load frame, a pair of 5 MP DIC cameras with 35 mm focal length lenses were used to capture the strain, curvature and 3D displacement data on both sides of the test coupons. Each pair of cameras was connected to a computer using Correlated Solutions Vic-3D software to process the image data. All systems were time-synchronized to enable the direct comparison of measurements.

B. Measurement of Bending Stiffness and Failure Curvature

For this testing, 15 bending coupons 50 mm long x 20 mm wide of the $[0_2/90_2/0_2]$ laminate described above were manufactured. Ten of these coupons were manufactured with the same fiber used for the sensors, but without FBGs inscribed. This yielded five samples each where the embedded fiber is located on the tensile or compressive side in bending. The remaining five samples were manufactured without any embedded fiber to provide a baseline comparison.

To minimize coupon variation induced by manufacturing, all of the coupons were cured simultaneously in three larger laminates, one for each testing group, that were then precisely cut down to the desired size to avoid possible edge effects. The central region of both sides of the coupons were speckled with white spray paint to create high contrast speckles for the DIC systems to track. These coupons were then mounted in the CBT fixture with a free length, or
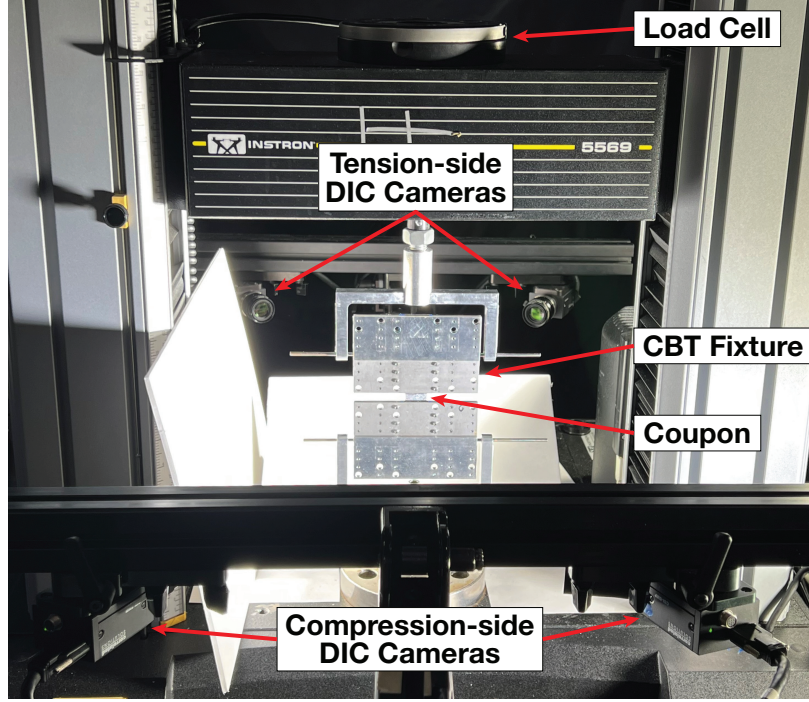
Fig. 3   Experimental setup.

coupon length between the fixture's rigid arms, of approximately 9 mm. This CBT fixture was equipped with thin polyimide tabs that extend slightly (1 mm) past the grips to help prevent premature failure at the grips due to local stress concentrations. Prior to each test, each sample was pre-conditioned by imposing a cross-head displacement of 10 mm (imposed curvature of < 100 m^{-1}) and holding it for 5-10 minutes. Each coupon was then bent until failure at a cross-head displacement rate of 10 mm/min. During each test, the force, displacement and time data were collected from the Instron at a rate of 4 Hz and both DIC systems captured images at a rate of 2 Hz. From the DIC data, the strain field, out-of-plane displacement, and curvature were all measured.

During the beginning part of the test while the laminate is undergoing elastic deformation, the moment and curvature follow a linear relationship from which the bending stiffness of the laminate, D_{11}, can be determined. Since the chosen laminate is a symmetric, balanced and cross-ply laminate, the B-matrix = 0 and the D-matrix portion of the ABD matrix has no bend-twist coupling ($D_{16} = D_{26} = 0$). Since the CBT fixture only imposes a moment in the longitudinal direction, M_x, ($M_y = M_{xy} = 0$) the relevant equation governing the bending of the coupons is

$$M_x = D_{11}\kappa_x + D_{12}\kappa_y \tag{3}$$

where the moment per unit width, M_x, that we measure, is related to both the longitudinal curvature, κ_x, and the transverse curvature, κ_y, by D_{11} and D_{12} respectively. For the chosen laminate, it can be assumed that $D_{11} \gg D_{12}$ and the κ_y measured during testing was 1-2 orders of magnitude smaller than κ_x enabling the second term of the equation to be neglected and the equation to be reduced to

$$M_x = D_{11}\kappa_x \tag{4}$$

where the bending stiffness D_{11} is the slope of the linear relationship between M_x and κ_x. M_x is the maximum moment in the coupon, which occurs at the center of the free length, and is calculated via

$$M_x = F(w + \Delta z) \tag{5}$$

where w is the maximum out-of-plane displacement in the center measured via DIC, Δz is the initial coupon offset from the load path, and F is the applied force per unit width. A free-body diagram of the CBT setup depicting this can be found in Fig. 4.
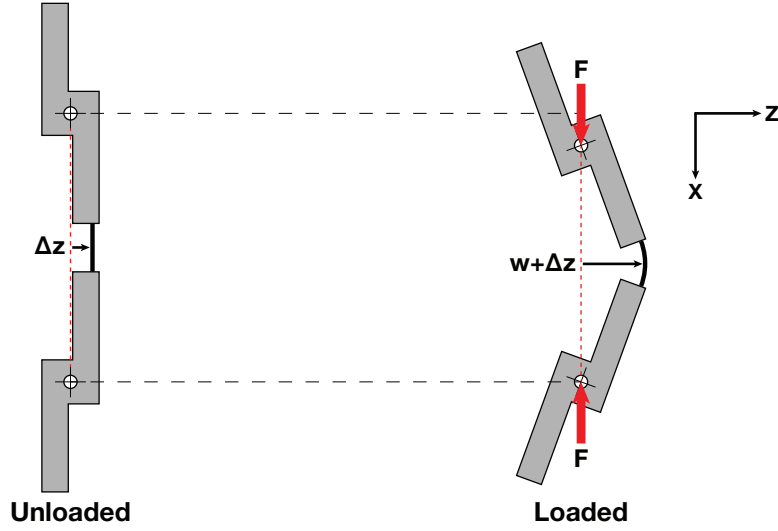
4

Fig. 4   Free-body diagram of CBT test layout.

The maximum curvature κ_x was also simultaneously measured and the slope of best linear fit between the M_x and κ_x measurements is D_{11} for that coupon. It was observed that at higher curvatures, the relationship between M_x and κ_x became nonlinear for all coupons, therefore the best linear fit was taken over the first minute of testing corresponding to a cross-head displacement of 10 mm and imposed curvature of < 100 m^{-1}. It was also observed that the first couple seconds of the test were also nonlinear and therefore the first five seconds of data were omitted in this fit. For all coupons, the calculated linear relationship had $R^2 > 0.99$ indicating a very good fit. The M_x vs κ_x curve for one of the coupons and the associated linear fit used to find D_{11} is shown in Fig. 5.

Fig. 5 M_x vs κ_x plot for one coupon.
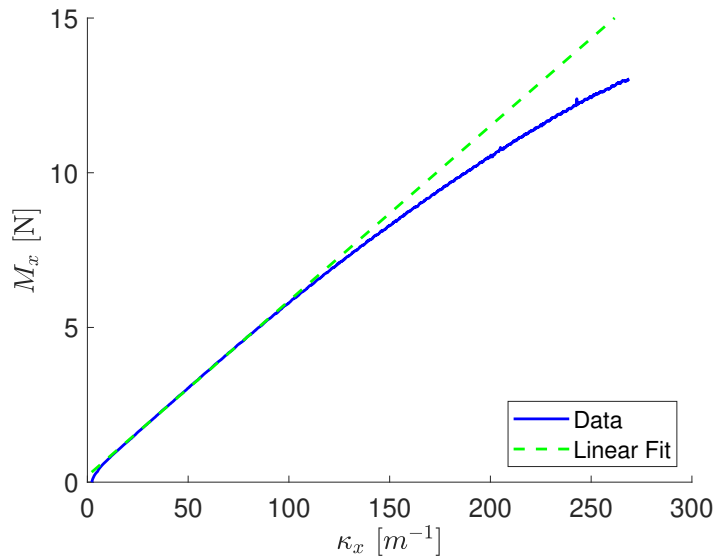
The curvature of the coupons was increased until they each failed, indicated by a drop in the applied force and typically an audible popping sound. The failure curvature $\kappa_{x,f}$ of each coupon was found by finding the maximum curvature at the center of the coupon corresponding to the first drop in applied force. An image of a failed coupon mounted in the CBT fixture is shown in Fig. 6.
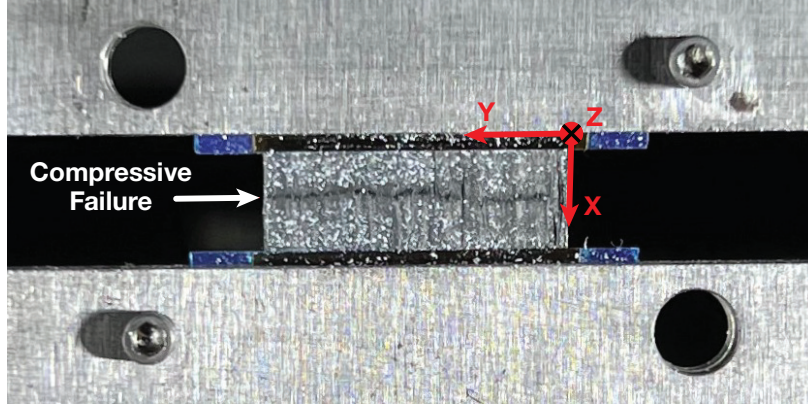
5

Fig. 6   Coupon failure on compression side.

C. Experimental Results

The mean and standard deviation of the results for all three test coupon groups are presented in Tables 1 and 2 for the bending stiffness D_{11} and failure curvature $\kappa_{x,f}$ respectively. The testing groups corresponding to the embedded FBG being on the tensile and compressive sides of the shell are denoted as $+F$ and $-F$ respectively. The control group without the embedded FBG is denoted NF. It is noted that these values were all calculated using the tensile side DIC data as it had the lowest uncertainty throughout testing.

Table 1   Bending Stiffness D_{11} [N-m])

	Mean	STD
+F	0.068	0.008
-F	0.066	0.008
NF	0.064	0.008

Table 2   Failure Curvature $\kappa_{x,f}$ [m^{-1}])

	Mean	STD
+F	227	18
-F	219	41
NF	217	54

In Table 1, it can be seen that for the particular laminate tested in this work the bending stiffness of the laminate does not appear to be affected by the inclusion of the fiber since the mean D_{11} value for all three testing groups are quite close together and all lie within each others' standard deviations. The same trend is observed for the failure curvature $\kappa_{x,f}$ in Table 2 which also showed no apparent dependence on fiber inclusion and/or position within the laminate. Both of these results make intuitive sense as the fiber makes up a relatively small fraction of the laminate with a diameter of just 30 μm while the entire laminate is 20 mm wide and approximately 200 μm thick. In terms of the failure of these laminates, it was observed that all coupons failed on the compression surface regardless of the inclusion of the fiber or its position within the laminate. μCT scans were taken near the failed regions of several coupons to observe how these laminates failed and to see if there were any indications of the failure initiating at the embedded fiber. Three cross-sections from these scans are presented in Figs. 7 - 9 alongside an image of the compression surface of the coupon of which the scan was taken.

In these three figures, we can see two main forms of damage: matrix cracks and delamination between the 0° and 90° lamina that are common between both the +F and -F coupons and occurred regardless if the fiber was present or not. It was observed that while cracks would gradually approach the embedded FBG as seen in Fig. 8 and eventually propagate around part of the sensor perimeter as seen in Fig. 7 there was no evidence of cracks initiating at the fiber
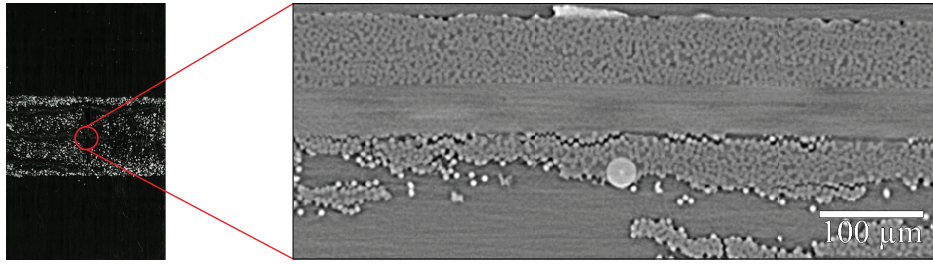
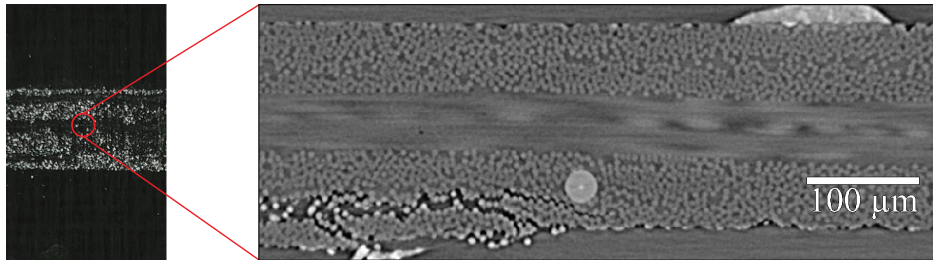**Fig. 7   -F coupon failure on compression side.**

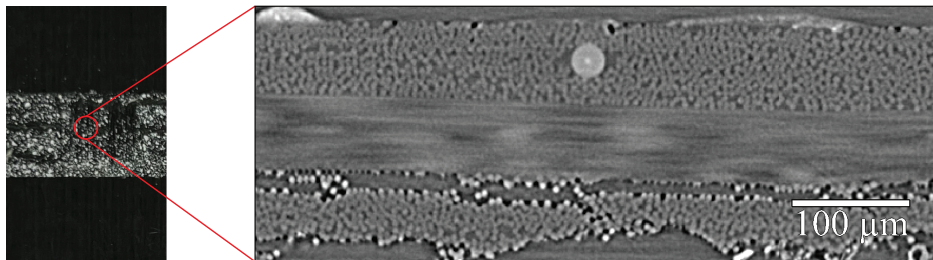**Fig. 8   Second -F coupon failure on compression side.**

Fig. 9   +F coupon failure on compression side

itself. Additionally, no failure was observed near the FBG in any of the scanned +F coupons, as seen in Fig. 9. This result aligns with our earlier finding that the embedment of the FBG sensors into the tested laminate appears to have no impact on its failure.

IV. Conclusions and Future Work

In this work we have presented recent progress towards the use of ultra-thin FBG sensors for the in-situ strain measurement of coilable thin composite shells. In the first part of this paper, a sensor with a 30 μm diameter was successfully embedded in a 200 μm thick laminate making it, to the best of our knowledge, the smallest FBG sensor that has been embedded in a composite laminate. Furthermore, it was demonstrated that FBG sensors constructed of this thin fiber could even be embedded in laminates down to 100 μm thick, further opening up the feasibility of using these sensors in coilable thin composite shells. In the second part of this paper, the column bending test was used to investigate if the inclusion of these sensors affects the bending behavior of the 200 μm thick laminate by measuring both the bending stiffness and failure curvature. The results of this testing indicate that for the particular laminate tested that the inclusion of the fiber and its position on either the tensile or compressive side had no effect on either of the measured bending properties. This conclusion was supported through μCT imaging of several of the failed samples which showed no indication of failure initiating at the embedded optical fiber.

Future work will focus on demonstrating the ability of these ultra-thin FBG sensors to accurately measure strain changes in coilable thin composite shells under bending. This will be done by subjecting these thin shells with embedded

FBG sensors to controlled bending experiments using the same CBT experimental setup described in Section III. These composites will be elastically bent and strain measurements from the FBG will be directly compared to a strain estimate at the fiber position using the through-thickness strain gradient obtained from DIC strain measurements on both surfaces of the laminate. This has the potential to enable a direct and accurate comparison to validate the strain measurements from these embedded FBGs before they are used to detect changes and damage in structures constructed out of these thin shells. Future work will also investigate how these embedded FBGs affect the mechanical performance of even thinner laminates than the one tested here. An example of such a laminate is depicted in Fig. 10 where a piece of the ultra-thin fiber was embedded in a laminate constructed of the same material used in this work but with a layup of [0/90/0] and approximate thickness of 100 μm.
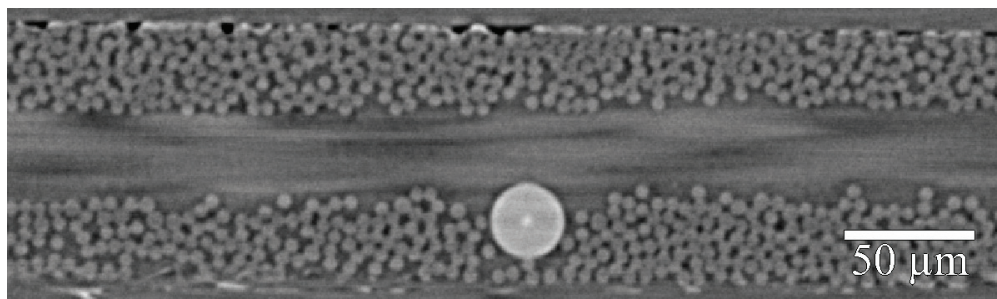

Fig. 10 μCT scan of [0/90/0] laminate with embedded fiber.

References

[1] Ubamanyu, K., Hasanyan, A. D., and Pellegrino, S., "Experimental Study of Time-dependent Failure of High Strain Composites," *AIAA SciTech Forum*, 2020. https://doi.org/10.2514/6.2020-0207.

[2] Wen, A., and Pellegrino, S., "Launch Vibration of Pre-Tensioned Coiled Structures," *AIAA SciTech Forum*, 2022. https://doi.org/10.2514/6.2022-1883.

[3] Takagaki, K., Minakuchi, S., and Takeda, N., "Process-induced strain and distortion in curved composites. Part I: Development of fiber-optic strain monitoring technique and analytical methods," *Composites Part A*, Vol. 103, 2017, pp. 236–251. https://doi.org/10.1016/j.compositesa.2017.09.020.

[4] Okabe, Y., Yashiro, S., Kosaka, T., and Takeda, N., "Detection of transverse cracks in CFRP composites using embedded fiber Bragg grating sensors," *Smart Materials and Structures*, Vol. 9, No. 6, 2000, pp. 832–838. https://doi.org/10.1088/0964-1726/9/6/313.

[5] Takeda, S., Minakuchi, S., Okabe, Y., and Takeda, N., "Delamination monitoring of laminated composites subjected to low-velocity impact using small-diameter FBG sensors," *Composites Part A*, Vol. 36, No. 7, 2005, pp. 903–908. https://doi.org/10.1016/j.compositesa.2004.12.005.

[6] Mulle, M., Zitoune, R., Collembet, F., Robert, L., and Grunevald, Y. H., "Measuring Strains through the Thickness of a Composite Structural Specimen Subjected to Bending," *Experimental Mechanics*, Vol. 49, No. 6, 2009, pp. 877–880. https://doi.org/10.1007/s11340-008-9209-2.

[7] Aller, B., Pellegrino, S., Kinkaid, N., Mejia-Ariza, J., Otis, R., Chan, P., and Pena, F., "Health Monitoring of High Strain Composites Using Embedded Fiber Bragg Grating Sensors," *AIAA SciTech Forum*, 2022. https://doi.org/10.2514/6.2022-1622.

[8] Takeda, N., Okabe, Y., Kuwahara, J., Kojima, S., and Ogisu, T., "Development of smart composite structures with small-diameter fiber Bragg grating sensors for damage detection: Quantitative evaluation of delamination length in CFRP laminates using Lamb wave sensing," *Composites Science and Technology*, Vol. 65, No. 15-16, 2005, pp. 2575–2587. https://doi.org/10.1016/j.compscitech.2005.07.014.